IOP Publishing Physica Scripta
Phys. Scr. **T132** (2008) 014053 (6pp) doi:10.1088/0031-8949/2008/T132/014053

Non-Boussinesq convection at moderate Rayleigh numbers in low temperature gaseous helium

A Sameen[1], **R Verzicco**[2] **and K R Sreenivasan**[1]

[1] International Centre for Theoretical Physics, Trieste 34014, Italy
[2] University of Roma, 'Tor Vergata', Italy

E-mail: krs@ictp.it

Received 4 November 2007
Accepted for publication 11 February 2008
Published 17 December 2008
Online at stacks.iop.org/PhysScr/T132/014053

Abstract
We study the effects of severe non-Boussinesq conditions on thermal convection at the moderate Rayleigh numbers of $Ra = 2 \times 10^8$ and 2×10^9 by resorting to direct numerical computations of the full governing equations. We illustrate the effects by considering low temperature gaseous helium. The properties of helium are allowed to depend on the temperature around the mean of 5.4 K. The Nusselt number is shown to decrease as the system departs from the Boussinesq approximation. For the Rayleigh numbers chosen here, the role of viscosity in thermal convection is limited to smudging the plume generation at the bottom surface, whereas the thermal expansion coefficient is demonstrated to have a larger impact on heat transport.

PACS numbers: 47.27.te, 47.55.P−, 47.55.pb, 47.27.ek

(Some figures in this article are in colour only in the electronic version.)

1. Introduction

The Rayleigh–Bénard system is a celebrated paradigm for convection in a variety of geophysical and engineering circumstances, such as the convection due to terrestrial heating by the Sun and convection in heat exchangers. In laboratory realizations of the Rayleigh–Bénard convection, the apparatus consists of a heated bottom horizontal plate and a cooled top horizontal plate, with the sidewalls essentially non-conducting. The aspect ratio is the relative size of the horizontal dimension of the apparatus with respect to the vertical distance between the horizontal plates. In applications, this ratio is often larger than unity.

The natural occurrence of thermal convection is associated with high Rayleigh number, defined as

$$Ra \equiv \frac{\alpha \Delta \Theta g H^3}{\nu \kappa}, \tag{1}$$

where α is the isobaric thermal expansion coefficient (or expansivity) of the fluid, $\Delta\Theta$ the temperature difference across the vertical distance H between the top and bottom plates, g the acceleration due to gravity, ν the kinematic viscosity and κ the thermal diffusivity of the fluid. The heat transport is measured by the Nusselt number, Nu, which is the ratio of the measured value to that possible only by thermal conduction. The Nusselt number is equal to unity in the absence of convection and increases with the Rayleigh number because of the onset of convection and, subsequently, of turbulence. At high enough Ra, it is generally assumed that Nu varies according to a power law in Ra: $Nu = ARa^{\beta}$ [1], or, sometimes, as a combination of power laws [2].

Existing theory for Rayleigh–Bénard convection is usually associated with the so-called Boussinesq conditions, according to which the density of the fluid is regarded as a constant except in so far as it affects the buoyancy term. In particular, fluid properties such as viscosity, thermal expansivity, thermal conductivity and specific heats are considered constants. The approximation is never perfectly true but is reasonably satisfactory when the temperature difference between the horizontal plates is small (in the sense that needs to be made more precise) [3]. It is a great simplification for both analytical theories (such as upper

bound estimates) and the numerical solutions of the governing equations.

The use of low-temperature helium gas in experiments has enabled very high Rayleigh numbers to be reached [4, 5]. Unfortunately, at the high end of Rayleigh number ranges covered by these experiments, the measured Nusselt numbers differ between experiments beyond measurement uncertainties. It has been argued that one possible explanation of this difference is the degree to which the Boussinesq approximation is valid. While some broad arguments were presented in [6], quantitative details have not yet been established.

This paper is devoted to quantitative considerations of the non-Boussinesq effects. We will attempt to understand the implications of Boussinesq approximation in Rayleigh–Bénard convection at moderate Ra by solving the full equations, and taking into account changes of fluid properties with temperature, for conditions that correspond to experiments with cryogenic helium gas. In keeping with the experimental situations, we consider a cylindrical domain. A notable effect of the departure from the Boussinesq approximation is the asymmetric temperature drop in the top and bottom boundary layers [7], though the related effect on Nu is speculative.

The following previous work on this topic must be mentioned. In [6], qualitative estimates were made to suggest that non-Boussinesq effects could be quite important. Ahlers *et al* [8] measured the Nu and center temperature, T_{cen}, for non-Boussinesq liquids. The corresponding measurements for gaseous thermal convection appeared in [9] with ethane as working fluid. The authors found that T_{cen} increases for liquids and decreases for gases, and reported that heat transport for gases increases considerably for severe non-Boussinesq condition: for ethane gas Nu_{nb} (where subscript 'nb' stands for non-Boussinesq) was found to be larger than Nu_{b} (the suffix 'b' standing for Boussinesq) by some ∼20% for $\alpha\Delta\Theta$ of 0.3. However, for water [8], the decrease in Nusselt number was marginal (∼1%). In [8], it was reported that the sum of thermal boundary layer thickness at top and bottom plates was approximately equal to twice the thermal boundary layer thickness obtained from Boussinesq conditions. Sujiyama *et al* [10] conclude from a two-dimensional non-Boussinesq computation for glycerol that this 'thickness sum rule' is applicable only to water.

2. Governing equation and computational method

The computational method used in the present paper is explained in detail in [11] and references cited there for a Boussinesq thermal convection. Only the changes made to accommodate non-Boussinesq effects are briefly described here. The governing equations in non-dimensional form under the low Mach number approximation read as

$$\frac{\partial \rho}{\partial t} + \nabla \cdot (\rho V) = 0, \tag{2}$$

$$\frac{\partial \rho V}{\partial t} + \nabla \cdot (\rho V V) = -\nabla p + \alpha T \hat{z} + \left(\frac{Pr}{Ra}\right)^{1/2} \nabla \times (2\mu S - \tfrac{2}{3}\mu(\nabla \cdot V) I), \tag{3}$$

$$\frac{\partial T}{\partial t} + \nabla \cdot (TV) = \left(\frac{1}{Pr\,Ra}\right)^{1/2} \frac{1}{\rho C_p} \nabla \cdot (\lambda \nabla T), \tag{4}$$

where S is the symmetric part of velocity gradient tensor. Here, we note that non-Boussinesq equation requires the physical properties to be temperature-dependent. The dynamic viscosity (μ), the density (ρ), the coefficient of thermal expansion (α), the constant pressure specific heat (C_p) and thermal conductivity (λ), appearing in the governing equation, are all non-dimensionalized by respective values at the mean temperature, Θ_0. The Rayleigh and Prandtl numbers are defined through values at Θ_0. As already remarked, we fix $\Theta_0 = 5.4$ K for all our computations.

The equations are non-dimensionalized by the free fall velocity $U = \sqrt{g\alpha\Delta\Theta H}$. The non-dimensional temperature is $T = (\Theta - \Theta_{\mathrm{c}})/\Delta\Theta$, where Θ is dimensional temperature of the convection system at any given point in space and time; $0 < T < 1$. The actual time-averaged temperature in the bulk is called T_{cen} which is different from the mean, $T_0 = (T_{\mathrm{h}} + T_{\mathrm{c}})/2$, due to the non-Boussinesq effect. The bottom plate is heated and kept at a constant temperature T_{h} and the top plate kept at T_{c}. The cylinder aspect ratio Γ is 1/2. The sidewall is taken to be adiabatic.

The equations are discretized on a staggered mesh by central second-order accurate finite-difference approximation, solved by a fractional-step procedure, with pressure equation inverted using trigonometric expansion in azimuthal direction and FISHPACK package [12] in the other two directions. The time marching is done with a third-order Runge–Kutta scheme [13, 14]. It should be noted that the velocity field is not divergence-free and that the compressibility of the gas is not accounted for. The vectors and scalars are staggered on space and time coordinates.

The time-discrete form for the temperature equation yields

$$T^{n+1} = T^n - \Delta t(BG^n + CG^{n-1}) + \left(\frac{1}{Ra\,Pr}\right)^{1/2} \frac{A\Delta t\kappa}{2} \nabla^2 (T^{n+1} + T^n), \tag{5}$$

where

$$G^n = \bar{V} \cdot \nabla T^n - \frac{\nabla \lambda^n \cdot \nabla T^n}{\rho^n C_p^n},$$

and A, B and C are coefficients of the time integration scheme, κ being the coefficient of thermal diffusion. The staggered time discretization will require V at t^{n+1}, which is extrapolated from t^n and t^{n-1} at the same time as T^n, to compute G^n. The implicitly treated diffusive term of the equation requires the values of thermal diffusivity at $t^{n+1/2}$, which is also extrapolated from values at t^n and t^{n-1}. Once the temperature field is computed, all properties are corrected using state equations. The momentum equation is discretized as

$$q^* = q^n - \Delta t(BH^n + CH^{n-1}) - A\Delta t \nabla p^n + \left(\frac{Pr}{Ra}\right)^{1/2} \frac{A\Delta t\mu}{2} \nabla^2 \left(\frac{q^*}{\rho} + \frac{q^n}{\rho^n}\right), \tag{6}$$

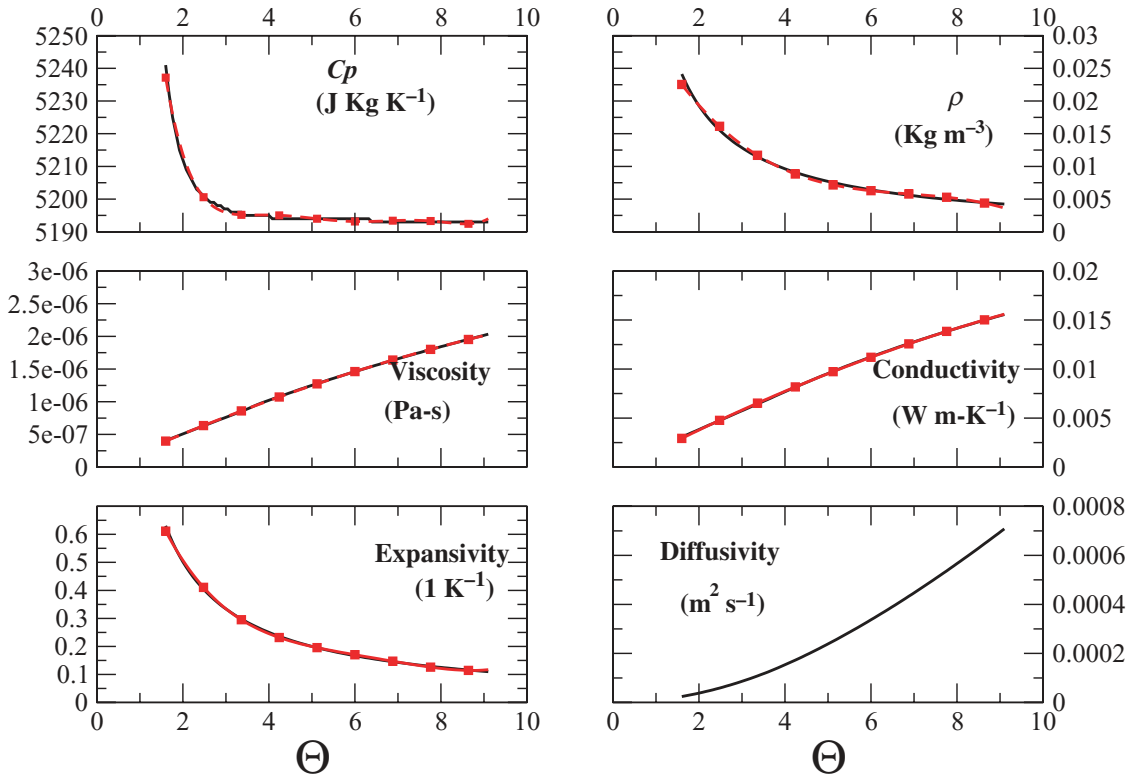

Figure 1. Properties computed from HEPACK (solid). The best-fit functions (dash-square) are used to evaluate the properties for the pressure and temperature ranges shown. The diffusivity variation in the bottom-right panel is from HEPAK calculations.

where

$$H^n = \nabla(q^n V^n) - \alpha T\hat{z} - \tfrac{1}{3}\mu\nabla(\nabla\cdot V^n) \\ -2S^n\cdot\nabla\mu + \tfrac{2}{3}(\nabla\cdot V^n)\nabla\mu.$$

Since the pressure at the latest time step is not known, we assume a surrogate momentum vector $q*$, with the error between q^{n+1} and $q*$ being given as $q^{n+1} - q* = -A\Delta t\nabla\phi$, where the scalar ϕ is computed from

$$\nabla^2\phi = \frac{1}{A\Delta t}\left(\nabla\cdot q^* + \frac{\partial\rho}{\partial t}\right); \qquad (7)$$

$\partial\rho/\partial t$ is evaluated at t^{n+1} from extrapolation of values computed from the continuity equation at t^n and t^{n-1}. The pressure is updated and the scheme is repeated for a new time step.

Simulations for $Ra = 2\times10^8$ and 2×10^9 reported here correspond to grid sizes of $97\times49\times193$ and $129\times65\times257$, respectively. These computational meshes can resolve the relevant smallest scales, as discussed in [11]. Nu is computed from the mean heat flux at the hot and cold plates as $Nu = \overline{\lambda\partial T/\partial z}|_w$, where the suffix w represents the derivative computed at the wall and the overbar represents average over time and a fixed horizontal plane.

The fluid under consideration is gaseous helium, whose properties are compiled by Cryodata Inc., in the package called HEPACK [15]. Table 1 shows the computed Prandtl number and Boussinesq parameter $\alpha\Delta\Theta$ for various operating pressures for Rayleigh number of 2×10^8 at $\Theta_0 = 5.4$ K. For each pressure, the properties are computed for a range of temperatures on either side of Θ_0 and the best-fit curve thus obtained is used as the temperature-dependent function of the corresponding property. The results for a sample pressure are shown in figure 1.

Table 1. Computed values of Prandtl number and Boussinesq parameter using HEPACK for $\Theta_0 = 5.4$ K evaluated for $Ra = 2\times10^8$.

P (Pa)	Pr	$\Delta\Theta(K)$	$\alpha\Delta\Theta$
80	0.6776	5.7073	1.05
90	0.6776	4.5104	0.83
110	0.6775	3.0176	0.56
180	0.6778	1.1264	0.20

One of the most commonly used parameters to determine Boussinesq condition is $\alpha\Delta\Theta$. For $\Theta_0 = 5.4$ K, various pressures produce different values of $\alpha\Delta\Theta$. The code is validated for the Boussinesq case, by fixing $\alpha\Delta\Theta = 0$ for $Ra = 2\times10^8$. The computed $Nu = 40.53\pm3.2$ matches well with the previous Boussinesq computation of $Nu = 41.32\pm2.3$ in [11]. For validating a non-Boussinesq case, we try to reproduce a case from [5] for $Ra = 5.8\times10^8$ and $Pr = 0.7$ for $\alpha\Delta\Theta = 1.11$ (one of the largest in the experiment), $\Theta_0 = 4.555$ K, $\rho_0 = 0.108$ kg m^{-3}. The experimental Nusselt number was 38.9. We could not quite reach $\alpha\Delta\Theta = 1.11$ because of numerical stability and limitation of available CPU time, but the comparison given in table 2 shows that the extrapolated result matches reasonably well with experiments.

3. Results and discussions

Figure 2 shows the variation of Nusselt number with respect to $\alpha\Delta\Theta$. There is a decrease in heat transport when the

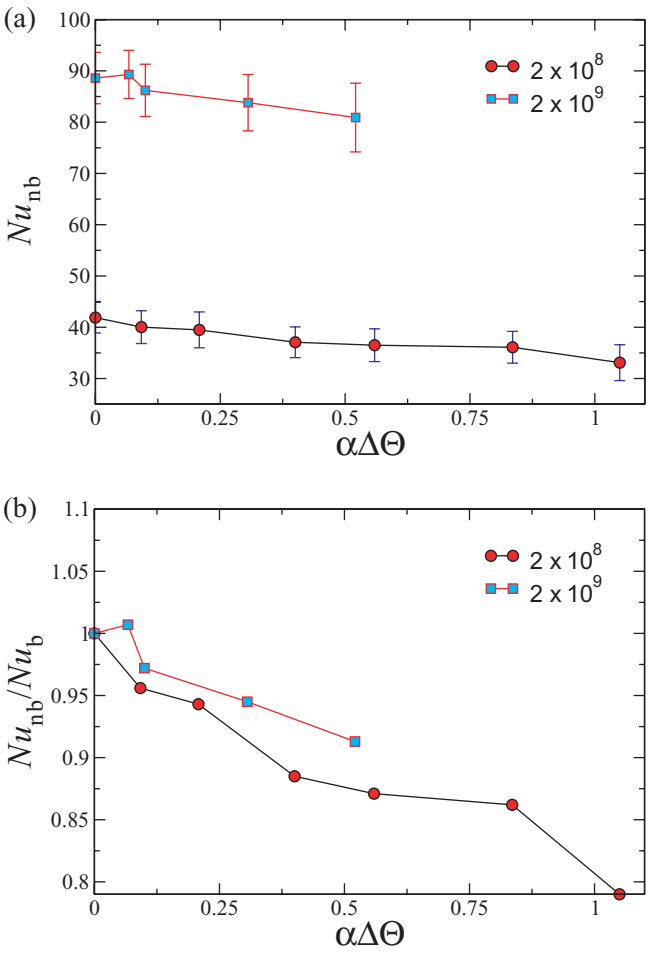

Figure 2. (a) Nusselt numbers variation against the non-Boussinesq parameter $\alpha\Delta\Theta$. (b) The Nusselt number ratio of the non-Boussinesq value to the Boussinesq value.

system departs from Boussinesq approximation. The decrease is more evident when the non-Boussinesq to Boussinesq ratio is plotted against $\alpha\Delta\Theta$ (figure 3(b)). Nusselt numbers for moderate to severe non-Boussinesq cases for these Rayleigh numbers are not studied systematically in the literature, except for a few data points from [5]. In figure 3, the experimental values of [5] are plotted, segregating (arbitrarily) those with $\alpha\Delta\Theta < 0.4$ from larger values, roughly treating them as representative of 'large' and 'moderate' non-Boussinesq effects. The computed values of the present DNS are shown as diamonds for $Ra = 2 \times 10^8$ and 2×10^9. The Nusselt number falls as the Boussinesq parameter increases. A heuristic explanation for this behavior is discussed below. At present, it is unclear if this decrease in Nu is 'universal'; in particular, it is not clear if the behavior can be sustained at much higher Rayleigh numbers.

Wu and Libchaber [7] demonstrated that an asymmetry in boundary layers between top and bottom walls will be generated due to non-Boussinesq conditions. The T_{cen} will then be different from the algebraic mean of top and bottom temperatures. Figure 4 shows that there is a reduction in the T_{cen} with increase in the Boussinesq parameter, $\alpha\Delta\Theta$. This is consistent with the experiments of [8, 9].

The thermal boundary layer thickness is plotted in figure 5. The figure shows that thermal boundary layer at the

Table 2. Nusselt number comparison of present computation with [5]. The experimental data correspond to $Ra = 5.38 \times 10^8$, $Pr = 0.7$ for $\alpha\Delta\Theta = 1.11$, $\Theta_0 = 4.555$ K and $\rho = 0.108\,\mathrm{kg\,m^{-3}}$.

$\alpha\Delta\Theta$	0	0.11	0.33	0.67	1.0
Nu	58	56.5	54	50.3	45

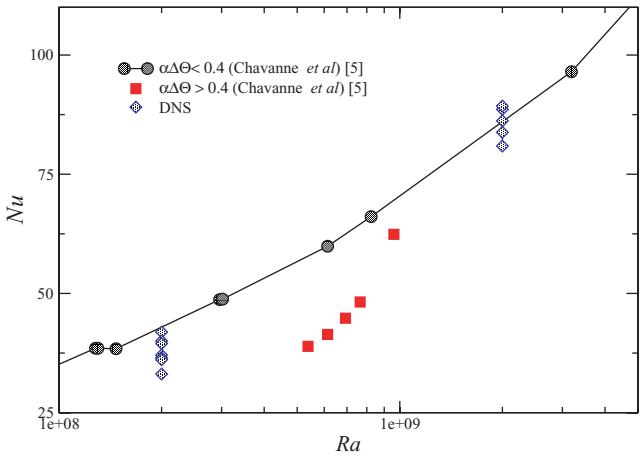

Figure 3. Comparison of the computed Nu with experimental values from [5]. The diamonds are the present DNS values whose $\alpha\Delta\Theta$ increases as the symbols move down in the ordinate (see table 1).

top is thinner than that at the bottom. In figure 6, we show the viscous boundary layer thickness against the Boussinesq parameter. The boundary layer thickness is defined here to be the distance of the peak root-mean-square value from the wall [11]. The sum of boundary layers of top and bottom are shown with square symbols, which is approximately equal to twice boundary layer thickness from Boussinesq computation:

$$\frac{2\delta_b}{\delta_{top} + \delta_{bottom}} \sim 1, \tag{8}$$

where the subscript 'b' stands for Boussinesq case, as before. At present, an explanation for this behavior is not known.

As shown in figure 5, the sum of top and bottom thermal boundary layer thickness increases with $\alpha\Delta\Theta$. This is consistent with two-dimensional computation of Sugiyama *et al* (see figure 5 of [10]) for glycerol: the sum decreases for low Rayleigh numbers ($\sim 10^4$) and increases for high Rayleigh numbers ($> 10^7$). Note that this sum rule does not apply as well to thermal boundary layers.

The obvious question is why the heat transport decreases with $\alpha\Delta\Theta$ for the Rayleigh numbers considered here. It is already known that there is large-scale circulation (the 'wind') for these Ra [11]. Consider $Ra = 2 \times 10^8$. In figure 7, the isosurfaces of temperature are shown for three different non-Boussinesq parameters. The contour values shown in the figure are 0.9 (red), 0.5 (green) and 0.1 (blue). From left to right they correspond to $\alpha\Delta\Theta = 0$, 0.56 and 1.05. The bulk flow in the Boussinesq case shows the wind with two counter rotating cells. As $\alpha\Delta\Theta$ increases, a big roll filling the entire height of the cell becomes more prominent. We infer that this is a manifestation of reduced heat transport and lower Nu. Figure 8 shows isosurfaces of axial velocity. The mixing of the fluid, thus the heat transfer, for $\alpha\Delta\Theta = 0$ (leftmost panel) is larger than that for $\alpha\Delta\Theta = 1.05$ (rightmost panel). To find the

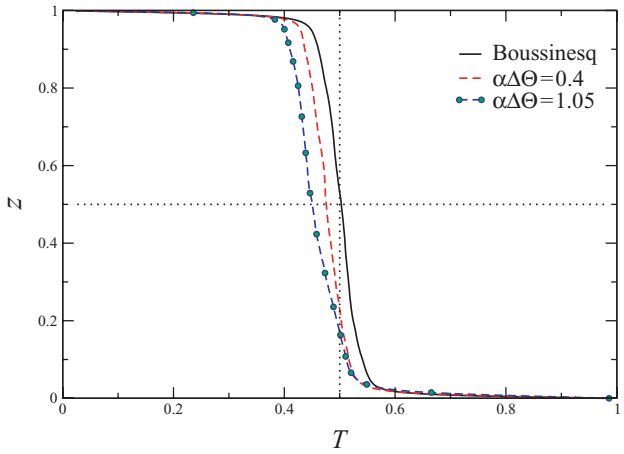

Figure 4. The average vertical temperature profile for various $\alpha\Delta\Theta$ for $Ra = 2 \times 10^8$ and $\Theta_0 = 5.4$ K.

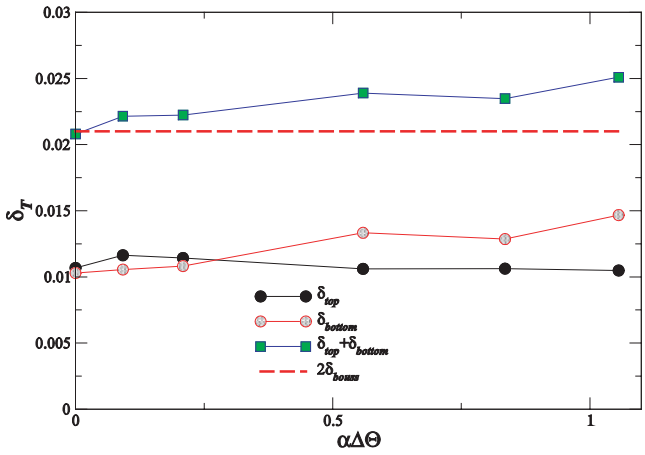

Figure 5. Temperature boundary layer thickness for $Ra = 2 \times 10^8$ and $\Theta_0 = 5.4$ K.

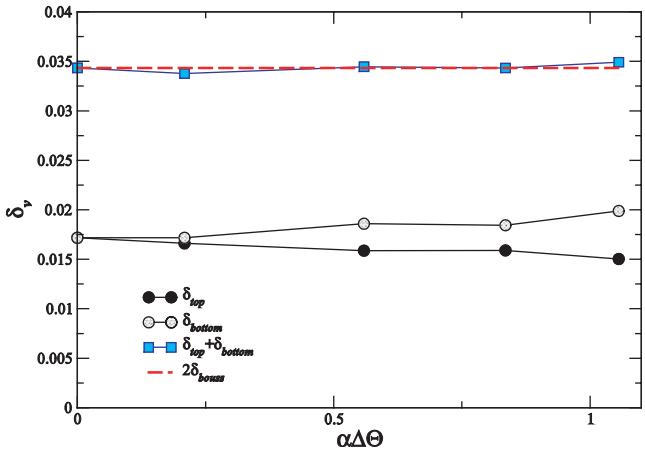

Figure 6. The boundary layer thickness for $Ra = 2 \times 10^8$ and $\Theta_0 = 5.4$ K. It is to be noted that $2\delta_b \approx \delta_{top} + \delta_{bottom}$.

reason for the decrease in mixing, we examine the generation of plumes.

At moderate Ra, our computations show major variations in conductivity, expansivity, viscosity and density within the thermal boundary layers. Of these quantities, conductivity and viscosity of helium increase with the temperature. This results in the bottom thermal boundary layer being thicker than that at

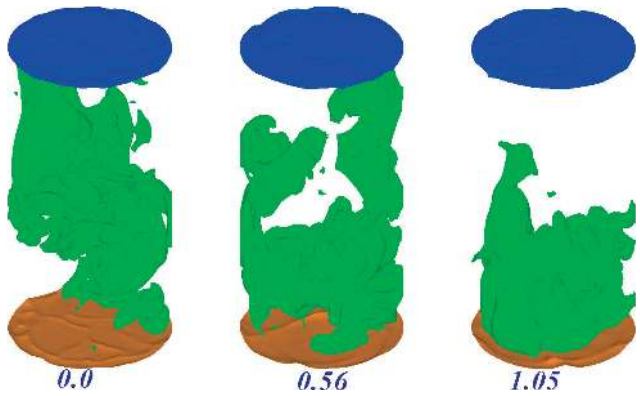

Figure 7. Instantaneous temperature isosurfaces for $T = 0.9$, 0.5 and 0.1, for $\alpha\Delta\Theta = 0$, 0.56 and 1.05.

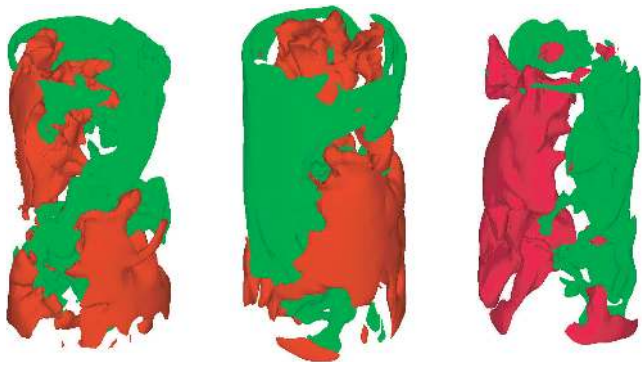

Figure 8. Instantaneous axial velocity isosurfaces for $v_z = -0.1$ and 0.1, for $\alpha\Delta\Theta = 0$, 0.56 and 1.05. The effective mixing decreases with increase in $\alpha\Delta\Theta$.

Figure 9. Instantaneous temperature isosurfaces (near the hot-bottom plate) for $T = 0.8$. From left to right, $\alpha\Delta\Theta = 0.0$, 0.56 and 1.05.

the top plate. We conjecture that the thermal plumes generated on the lower plate are smeared out by the larger viscosity in the vicinity. This means that fewer plumes from the lower plate rise all the way to the top (figure 9). In effect, the heat transport to the bulk is hindered by the highly viscous and conducting bottom thermal boundary layer. The reverse happens in the top boundary layer and convection through jets dominates the heat transfer, but, since the temperature at mid-height is lower than T_0, the heat transport by jets is not large enough to compensate the reduction from the bottom plate.

To further elucidate the roles of various fluid properties on global heat transport, we repeat the calculations as follows. The dominance of property X can be identified by computing with $X = f(T)$, while holding all other properties constant. Table 3 shows the computed Nusselt numbers for such hypothetical cases. It is clear that expansivity has the largest effect on heat transport. In figures 10 and 11, temperature isosurfaces near top and bottom plates are shown for $\alpha\Delta\Theta = 1.05$, while only μ and α are individually allowed to vary. As mentioned earlier, the role of viscosity is to smear out

Table 3. Contribution of each property variation to heat transport. First column is the Nusselt number obtained from the Boussinesq computation, and second column from full non-Boussinesq computation. Nusselt numbers calculated when each property, X, is alone allowed to depend on the temperature are also shown.

	Bouss	Non-B	$X=\mu$	$X=\alpha$	$X=C_p$	$X=\lambda$	$X=\rho$
Nu	40.53	33.1	38.5	33.6	40.4	39.2	38

Figure 10. Temperature isosurfaces for $T = 0.8$. The leftmost panel is for the non-Boussinesq case when all properties are allowed to depend on temperature; the middle panel corresponds to viscosity alone being a function of temperature; the right panel corresponds to the case for which the expansivity alone is a function of temperature.

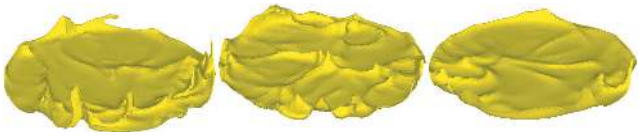

Figure 11. Same as figure 10 but with isosurface values 0.2.

the plume generation, but the Nusselt number is reduced only marginally. However, when only the expansivity is allowed to depend on the temperature, the Nusselt number is reduced dramatically, even though the plumes generated are about the same as the Boussinesq case. Thermal expansivity determines the volume increase of a parcel of fluid due to temperature changes. Since expansivity has a negative dependence on temperature, a parcel of fluid moving up from the bottom will increase in volume dramatically in comparison to the Boussinesq case. This will lead to an increase in the surface area available for conduction, thus promoting local exchange while reducing transport to the top plate. In effect, this reduces the Nusselt number.

4. Conclusions

The non-Boussinesq effect in thermal convection is investigated by direct numerical simulation of the full governing equations. The non-dimensional heat transport, or the Nusselt number, is found to decrease nearly 20% for the severely non-Boussinesq case of $\alpha\Delta\Theta \approx 1$. The conclusion of [9] that for gases Nu increases with increase in $\alpha\Delta\Theta$ is thus not general. We have shown that viscosity plays a moderately important role in diminishing the movement of plumes to the interior of convection domain by smearing out the generation at the hot plate. The coefficient of thermal expansion, because of negative dependence on temperature, subjugates thermal convection by increasing the effective surface area available for conduction. This enhances the local heat transfer, reduces the amount transmitted to the top wall, and thus the Nusselt number. These conclusions are specific to gaseous helium and the conditions chosen, since a qualitatively different property variation may lead to a different conclusion. For example, near the critical point, where most high Rayleigh numbers are experimentally achieved, the specific heat is highly sensitive to temperature, which can make the global heat transport dramatically different. In particular, the results will depend on the path by which one approaches the critical point. At present, we are not in a position to comment generally on all non-Boussinesq effects, especially at very high Rayleigh numbers.

Acknowledgment

We thank J J Niemela for useful discussions and for lending us the HEPACK package.

References

[1] Malkus M V R 1954 Heat transport and spectrum of thermal turbulence *Proc. R. Soc. Lond.* A **225** 196–212
[2] Grossmann S and Lohse D 2000 Scaling in thermal convection: a unifying view *J. Fluid Mech.* **407** 27–56
[3] Tritton D J 1988 *Physical Fluid Dynamics* 2nd edn (Oxford: Clarendon)
[4] Niemela J J, Skrbek L, Sreenivasan K R and Donnelly R J 2000 Turbulent convection at very high Rayleigh numbers *Nature* **404** 837–40
[5] Chavanne X, Chilla F, Chabaud B, Castaing B and Hebral B 2001 Turbulent Rayleigh–Benard convection in gaseous and liquid He *Phys. Fluids* **13** 1300–20
[6] Niemela J J and Sreenivasan K R 2003 Confined turbulent convection *J. Fluid Mech.* **481** 355–84
[7] Wu X-Z and Libchaber A 1991 Non-Boussinesq effects in free thermal convection *Phys. Rev.* A **43** 2833–9
[8] Ahlers G, Brown E, Araujo F F, Funschilling D, Grossmann S and Lohse D 2006 Non-Oberbeck–Boussinesq effects in strongly turbulent Rayleigh–Benard convection *J. Fluid Mech.* **569** 409–45
[9] Ahlers G, Araujo F F, Funschilling D, Grossmann S and Lohse D 2007 Non-Oberbeck–Boussinesq effects in gaseous Rayleigh–Benard convection *Phys. Rev. Lett.* **98** 054501
[10] Sugiyama K, Calzavarini E, Grossmann S and Lohse D 2007 Non-Oberbeck–Boussinesq effects in two-dimensional Rayleigh–Bénard convection in glycerol *Europhys. Lett.* **80** 34002
[11] Verzicco R and Camussi R 2003 Numerical experiments on strongly turbulent thermal convection in a slender cylindrical cell *J. Fluid Mech.* **477** 19–49
[12] Swartzrauber P N 1974 A direct method for the discrete solution of separable elliptic equations *SIAM J. Numer. Anal.* **11** 1136–50
[13] Verzicco R and Camussi R 1997 Transitional regimes of low-Prandtl thermal convection in a cylindrical cell *Phys. Fluids* **9** 1287–95
[14] Verzicco R and Orlandi P 1996 A finite-difference scheme for three-dimensional incompressible flow in cylindrical coordinates *J. Comput. Phys.* **123** 402–13
[15] Arp V D and McCarty R D 1998 The properties of critical helium gas *Technical report* University of Oregon